CrystEngComm

ROYAL SOCIETY OF CHEMISTRY

PAPER

View Article Online
View Journal | View Issue

Cite this: *CrystEngComm*, 2021, **23**, 5876

Light-fueled rapid macroscopic motion of a green fluorescent organic crystal†

Prasenjit Giri,[a] Abhrojyoti Mazumder,[a] Dibyendu Dey,[a] Souvik Garani,[a] Anju Raveendran[b] and Manas K. Panda *[a]

Received 6th April 2021,
Accepted 7th May 2021

DOI: 10.1039/d1ce00460c

rsc.li/crystengcomm

We report here a new green fluorescent organic crystal of an amide functionalized acrylonitrile derivative (***E*-ArF$_2$**) that displays various types of macroscopic response when illuminated with UV light (390 nm). The shape deformation and actuation of the ***E*-ArF$_2$** crystal can be controlled on-demand by shining UV-light on the specific parts of the crystal and reversing the direction of light illumination. When UV light is shone on the (001) face of a straight crystal, it rapidly bends away from the light source and can be bent to the opposite direction by reversing the illumination direction on the other face (00–1). With the aid of various analytical techniques, NMR, IR, UV-vis and X-ray diffraction, we established that the light fueled macroscopic actuation of the ***E*-ArF$_2$** crystal is rooted to the combined effect of *E*- to *Z*-isomerization and the [2 + 2] cycloaddition reaction in the solid state. Based on the above experimental facts, a general mechanistic model of the actuation is also proposed.

Introduction

Smart responsive materials that are capable of transforming light, heat, pressure or hygro stimuli into macroscopic motion are of immense importance in fundamental and technological research.[1–12] Among the various stimuli generally being used, light has special importance because of the advantage that it can be remotely controlled to manipulate the properties of the material. Certain molecular crystals have extraordinary ability to transform light-triggered molecular motion into macroscopic actuation[13–20] and thus can be used in soft robotics, machinery devices, medical devices, artificial muscles, *etc.* It is notable to mention here that molecular cooperativity is important to amplify such nanoscopic molecular motion into macroscopic actuation. Among various reports of such molecular crystals (organic/metal–organic), the majority of them contain azobenzene,[21–25] anthracene,[26–28] salicylidenephenylethylamines,[29,30] a styryl benzene ring,[31–36] and diarylethene[37,38] molecules as the photoactive functional group and are capable of displaying macroscopic actuation when UV light is shone on them. The macroscopic motions in these crystals are rooted to photo-induced geometric isomerization, photocycloaddition, ring-opening/closing reactions, phase transitions, *etc.* that occur in the light illuminated surface and thereby generating a bimorphic strain that drives the crystal shape deformation followed by actuation. Recently, a new class of crystals based on acylhydrazone molecules that exhibit photomechanical actuation is reported.[39,40] However, to our knowledge, reports on photomechanical crystals based on a cyanovinyl-derivative are really scarce and there exist only a few examples of cyanovinyl-based molecules that exhibit photoinduced bending.[41–43]

Achieving precise control of crystal motion or rapid and on-demand shape deformation using light stimuli remains a formidable challenge. Thus, there is a long-standing demand to develop new molecular materials equipped with light-responsive functionality and suitable intermolecular interactions that can exhibit a delicate interplay between light-responsivity and crystal elasticity for rapid and controllable actuation. A rational approach *via* molecular design and crystal engineering is necessary to develop efficient photo-responsive crystals.

Herein, we report a new class of fluorescent organic crystals based on an amide functionalized cyanovinyl derivative (***E*-ArF$_2$**) that displays rapid and on-demand shape deformation in the presence of UV light (390 nm). The molecule contains an amide functional group that is engaged in intermolecular H-bonding interactions while the π–π stacking interaction between the phenyl rings effectively brings the acrylonitrile double bond within the critical distance for [2 + 2] photo-cycloaddition reaction in the solid-state (Schmidt criteria 4.2 Å). The actuation of the ***E*-ArF$_2$**

[a] *Department of Chemistry, Jadavpur University, Kolkata-700032, India. E-mail: mannup25@gmail.com, manaspanda.chemistry@jadavpuruniversity.in*
[b] *KAHM Unity Women's College, Narukara, Mallapuram, Kerala-676122, India*

† Electronic supplementary information (ESI) available: Actuation videos, experimental details, ^{1}H and ^{13}C NMR data, mass spectra, X-ray crystallographic data, UV-vis/fluorescence spectral data, TGA, and packing diagrams. CCDC 2075638. For ESI and crystallographic data in CIF or other electronic format see DOI: 10.1039/d1ce00460c

crystal can be precisely controlled by irradiating light on the specific position of the crystal surface or by changing the illumination direction. We establish that the actuation of the ***E*-ArF$_2$** crystal is a macroscopic manifestation of light-fueled *E*- to *Z*-isomerization and the [2 + 2] cycloaddition reaction in the solid-state.

Compound ***E*-ArF$_2$** was synthesized by Knoevenagel condensation between 4-acetamido benzaldehyde and 3,5-difluorophenylacetonitrile in the presence of potassium *tert*-butoxide as a base (85% yield, Scheme S1, ESI†). The compound was thoroughly characterized by ^{1}H NMR, ^{13}C NMR, and mass spectrometry (Fig. S1–S3, ESI†). Thermogravimetric analysis suggests that the compound is thermally stable up to 250 °C (Fig. S4, ESI†). Crystallization of the compound from DMF solution provides long acicular crystals along with several thin ribbon-shaped crystals, some of which are inherently bent. The molecular structure of the crystal was confirmed by single crystal X-ray diffraction which reveals the *trans* geometry of two aromatic rings around the acrylonitrile bond (Fig. 1c). When observed under a fluorescence microscope, needle shaped pristine crystals of ***E*-ArF$_2$** emit green light ($\lambda_{em,max}$ = 503 nm, $\phi_{crystal}$ = 0.03, Fig. 1b). The ***E*-ArF$_2$** compound does not show any visually detectable AIE effect in solution (THF : water mixture). Thus, the green fluorescence of the ***E*-ArF$_2$** crystal could be attributed to the crystallization induced emission enhancement (CIEE).[44,45] These green fluorescent crystals start actuating immediately after UV light illumination (365 nm UV light, Movie S1†) under the microscope. Various types of kinematic motion like bending, rolling, and flipping were observed under UV-light from a fluorescence microscope (Fig. 1e and f and Movies S2–S4†). This actuation can be ascribed to photoinduced *E* to *Z*-isomerization around the double bond of the ***E*-ARF$_2$** molecule in the solid crystal. On heating the photo-bent crystal at 100 °C for 6 hours, it slowly returned to nearly its original straight shape (Fig. S5, ESI†) and can be actuated again by UV light irradiation under a microscope. To our knowledge, this is the first example of an acrylonitrile based organic crystal which shows optical response (*i.e.* green fluorescence) as well as mechanical response (*i.e.* macroscopic actuation) in the presence a single stimulus, *i.e.* UV light.

Observation under a fluorescence microscope motivated us to investigate the crystal actuation properties in more details and in a systematic manner. To do this, the crystal was placed on a glass slide under the microscope attached with a camera and the video of crystal actuation upon light illumination was recorded. When a thin fibre shaped crystal of ***E*-ArF$_2$** was irradiated with 390 nm light (torch light, power density 5 mW) on the wider (001) face, the crystal instantaneously bends away from the light source. The shape deformation can be manipulated by controlling the illumination at different positions of the crystal. As shown in Fig. 2a–f and Movie S5,† the straight crystal can be gradually bent by a flash of UV light at the specific position on the crystal surface (shown by arrow) and the deflection angle is changed from 0° → 56° → 88° → 142° → 155° and finally reaches its maximum at ~202° forming a U-shape. As observed under an optical microscope, the U-shaped crystal retained its macroscopic integrity without the formation of any crack or fracture on the surface. As shown in Fig. S6, ESI,† the SEM images showed no change in the surface

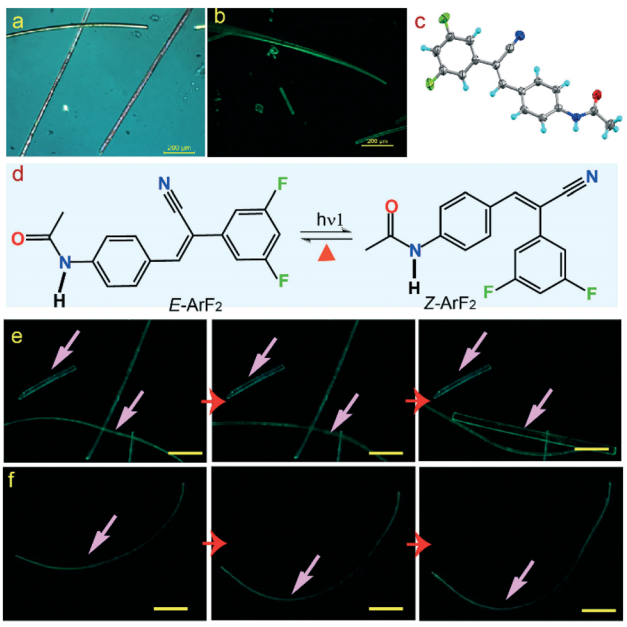

Fig. 1 (a) Optical microscope image of the ***E*-ArF$_2$** crystal, (b) image of the ***E*-ArF$_2$** crystal showing green fluorescence, (c) molecular structure of ***E*-ArF$_2$** showing *trans*-geometry, (d) schematic diagram of *E*- to *Z*-isomerization upon UV irradiation, and (e and f) photomechanical actuation of the green fluorescent ***E*-ArF$_2$** crystal under a fluorescence microscope. Snapshots were taken from Movies S2 and S4, ESI.†

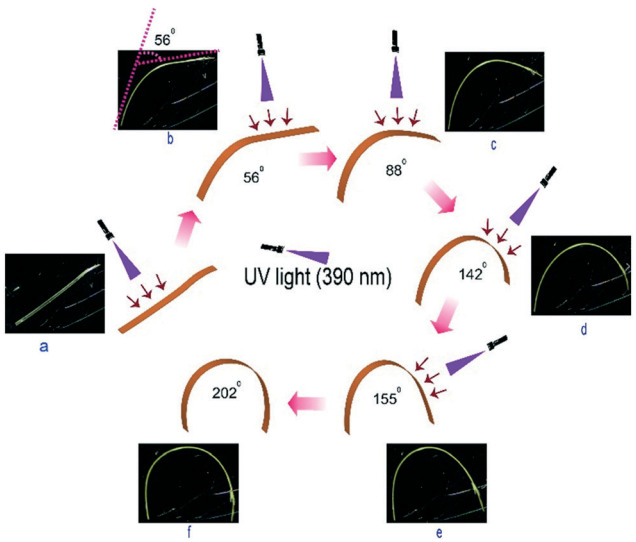

Fig. 2 (a–f) Stepwise and controlled bending of a straight ***E*-ARF$_2$** crystal to a U-shape by light irradiation (390 nm) at specific positions. The change in deflection angles is given and the maximum deflection angle of 202° was attained at the bent "U" shape. The image snapshots were extracted from Movie S5, ESI.†

morphology of the crystal surface after the 1st cycle of photomechanical bending.

In another experiment, when a thin ribbon-shaped bent crystal was irradiated with UV light at the terminal of the (001) face, the crystal readily bent to form a "hook" shape (as shown in Fig. 3a, Movie S6†). After irradiation at a specific position (shown by arrows) at the other terminal of the opposite face (00−1), the crystal continues to deform to adopt an "S" shape (Fig. 3a–d). Accordingly, the bending angles at the two terminals are calculated to be 120° and 161°. This movie demonstrates that the crystal can be deformed to its desired shape by judicious selection of the illumination area on the crystal surface and the direction of illumination.

Interestingly, the crystal can be returned to its nearly original straight shape by reversing the irradiation face (as shown by arrows, Fig. 3e–g). However, this shape-reversibility can be repeated up to two cycles only, after which the crystal motion significantly slowed down indicating the deterioration of crystal elasticity and integrity upon repeated and prolonged photoirradiation presumably because of [2 + 2] photocycloaddition in addition to *E–Z* isomerization. We demonstrate here that the light fuelled deformation of the crystal can be precisely controlled by manipulating the irradiation location (on the crystal surface) and the direction of illumination. Such precise control of light irradiation to achieve a desired shape change is unique to our ***E*-ArF$_2$** crystal and not very common in the literature. Apart from these, several other crystals having different dimensions and shapes have been examined for photomechanical actuation and are shown in Movies S7–S10, ESI.†

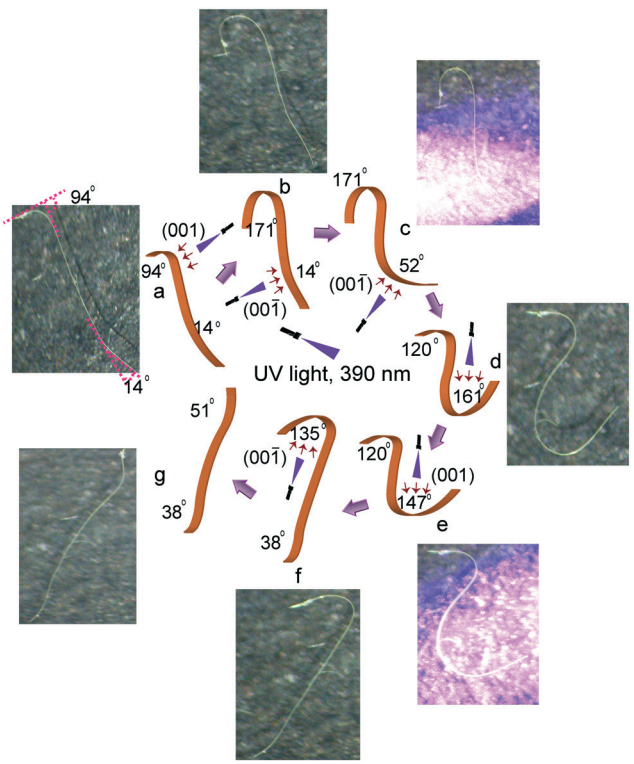

Fig. 3 (a–d) The gradual bending of a thin ribbon-shaped crystal to an S-shape upon UV light irradiation on the (001) and (00–1) face, (e–g) unbending of the bent crystal by reversing the illumination direction. The change in shape and bending angles is shown by cartoon representation. The snapshots of the crystal were extracted from Movie S6, ESI.†

To obtain better insight into the molecular packing and intermolecular interaction, we have carried out single crystal X-ray diffraction of the ***E*-ArF$_2$** crystal. Slow evaporation of the compound from DMF solution yielded cuboid shaped orthorhombic crystals with the $P2_12_12_1$ space group (Table S1, figure ESI†). The molecules in the lattice are stabilized by several intermolecular H-bonding interactions involving (O═C) N–H···NC, H_2C–H···NC, and (NH)C═O···H groups as well as π–π stacking interactions which play an essential role in maintaining crystal integrity during photomechanical bending (Fig. 4b). The carbonyl oxygen of the amide group is connected to two neighbouring antiparallel molecules involving a trifurcated H-bonding interaction (H···A distances are 2.491 Å, 2.593 Å and 2.689 Å) which is extended along the *b*-axis of the crystal. The nitrogen atom of the CN group also engaged in bifurcated H-bonding interaction (H···A distance 2.675 Å) with the C–H and N–H protons of the neighbouring molecule. Both the phenyl rings of the ***E*-ArF$_2$** molecule are engaged in π–π stacking interaction in a parallel fashion (centroid to centroid distance 3.871 Å) which is extended along the length (||*a*-axis) of the crystal (Fig. 4c). This interaction plays an important role in maintaining the crystal integrity during the photomechanical bending. The π–π stacking of the aromatic rings brings the vinylidene double bonds of two neighbouring molecules within the distance of 3.871 Å which is smaller than 4.2 Å and the obtuse angle (<C8–C7–C7′) between these double bonds is 98.67° (Fig. 4c and S7, ESI†) and thus, according to Schmidt's criteria this double bond is susceptible to photodimerization reaction in the solid crystal.[46,47] In fact, as mentioned earlier, prolonged or repeated UV irradiation of the crystal leads to a small fraction of the [2 + 2] cycloaddition product (Fig. S8 and S9, ESI†). The packing

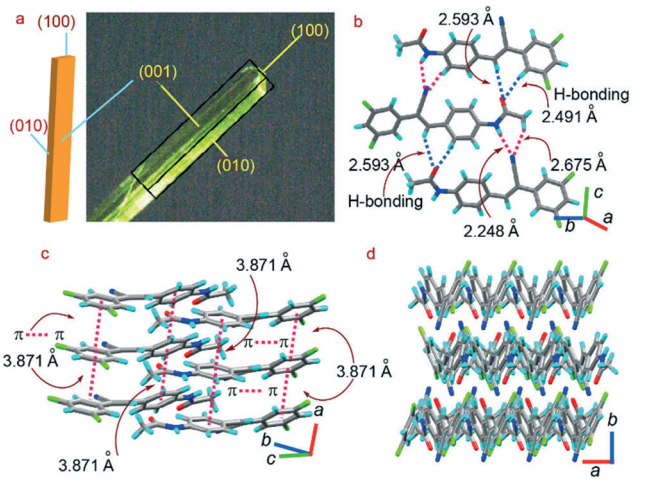

Fig. 4 (a). Face indexing of the ***E*-ArF$_2$** crystal, (b) hydrogen bonding interactions involving C–H···O and C–H···N synthons, (c) π–π stacking interactions and (d) molecular packing viewed along the *c*-axis.

arrangement of molecules in the ***E*-ArF$_2$** crystal is shown in Fig. 4d and S10–S12, ESI.† Despite our repeated attempts we were unsuccessful in obtaining a good quality crystal of the photoproduct (photo-irradiated crystal) for X-ray diffraction.

To understand the molecular level changes of the macroscopic actuation of the ***E*-ArF$_2$** crystal, we have carried out ^{1}H NMR, UV-vis, PXRD and IR spectroscopy. As observed from the ^{1}H NMR spectra of ***E*-ArF$_2$** (in DMSO-d_6 solution), the chemical shift of –N*H* protons at 10.38 ppm in the *E*-isomer is shifted to the high-field region at 10.32 ppm that corresponds to the *Z*-isomer upon photoirradiation (390 nm LED light, 1 mW, Fig. 5a). Similarly, the proton of the C*H*═C moiety shifted from 8.2 ppm in the *E*-isomer to 7.7 ppm in the *Z*-isomer. By comparing the intensities of N*H* proton peaks, 71% conversion was observed in 5 minutes of UV-irradiation in solution. Longer irradiation of the solution leads to the [2 + 2] cycloaddition product after which no change of peak intensity was observed indicating the attainment of the photostationary state in solution. This photochemical behaviour is slightly different in the solid state. To observe this, ***E*-ArF$_2$** crystals were irradiated with UV light (390 nm, 5 mW cm^{-2}) for 5 minutes, and subsequently dissolved in DMSO-d_6 and ^{1}H NMR spectra were recorded. As observed in the ^{1}H NMR spectra in Fig. S8, ESI,† a mixture of the photo-isomerized product (major) and photo-dimerized (minor) products was obtained. Two different proton peaks in the region of 5–6 ppm could be attributed to two different cyclobutane rings which indicates the possibility of the [2 + 2] cycloaddition reaction occurring in both the *E*- and photo-converted *Z*-isomer. Mass spectra of the same solution showed a distinct peak at *m*/*z* 597.157 that corresponds to the [2 + 2] cycloaddition product and corroborates with the above observation (Fig. S9, ESI†). Thus, crystal actuation under UV light is presumably due to the combined effect of geometric isomerization and the [2 + 2] cycloaddition reaction in the solid-state.

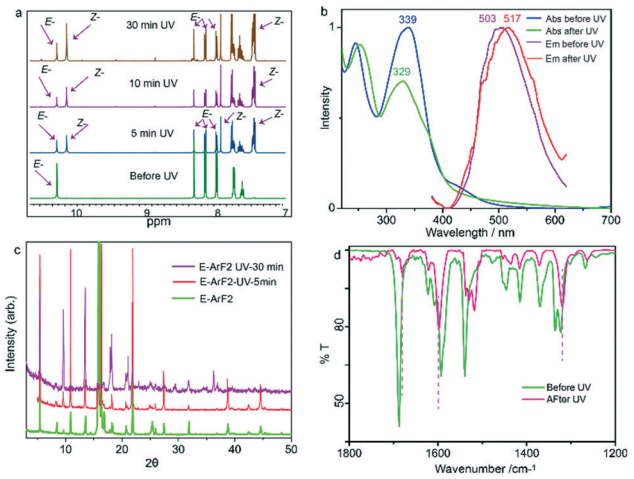

Fig. 5 (a). ^{1}H NMR (DMSO-d_6 solution) spectra of ***E*-ArF$_2$** before and after UV irradiation, (b) solid-state UV-vis and fluorescence spectra of ***E*-ArF$_2$** before and after UV irradiation, (c) PXRD of ***E*-ArF$_2$** before and after UV irradiation, and (d) IR spectra of ***E*-ArF$_2$** before and after UV irradiation.

UV-vis spectra of ***E*-ArF$_2$** in DMF solution (1×10^{-5} M) exhibit two distinct absorption bands at 353 nm (λ_{max}) and 234 nm which when irradiated with UV light (390 nm) shifted to 343 nm and 244 nm, respectively (Fig. S13, ESI†). Accordingly, solid-state absorption bands of ***E*-ArF$_2$** also shifted from 339 nm and 244 nm to 329 and 253 nm, respectively, upon irradiation (Fig. 5b). The solid-state fluorescence maxima (λ_{max}) of the crystal change from 503 nm to 517 nm after irradiation. This change is attributed to the photoinduced *E*- to *Z*-isomerization in the solid crystal of ***E*-ArF$_2$**.

To see the change in supramolecular packing during photomechanical actuation, PXRD of ***E*-ArF$_2$** was carried out before and after irradiation. As shown in Fig. S14, ESI,† the experimental PXRD pattern of ***E*-ArF$_2$** matches well with the simulated pattern (obtained from single crystal X-ray diffraction data using Mercury software). The peak intensity of ***E*-ARF$_2$** gradually decreases with increasing the time of UV irradiation (Fig. 5c) suggesting the loss of the degree of crystallinity that could be associated with the [2 + 2] cycloaddition product formed by longer UV irradiation. In order to obtain the change in bond strength and associated non-covalent intermolecular interactions during photoisomerization, infrared spectra were recorded before and after UV irradiation (Fig. 5d and S15, ESI†). As observed from Fig. 5d, the stretching frequencies of both C═O (amide-1) and N–H in plane bending (amide-II) shifted from 1689 cm^{-1} and 1539 cm^{-1} to 1638 cm^{-1} and 1517 cm^{-1}, respectively, after UV irradiation. A notable change in peak shape was also observed. This suggests a significant change in symmetry of the molecule and the mode of non-covalent interactions associated with these bonds. In contrast to the red shift of the amide-I and amide-II frequency, the C═C stretching frequency showed a blue shift from 1593 cm^{-1} to 1597 cm^{-1} upon UV irradiation. A significant shift in the aromatic C–H bending frequencies at 1338, 1322 and 1122 cm^{-1} was observed upon UV illumination suggesting the reconfiguration of H-bonding interaction involving the (Ar)C–H bond during the photoreaction process.

To obtain an overall picture of the photomechanical motion of the ***E*-ArF$_2$** crystal we have developed a plausible mechanistic model which is shown in Fig. 6. The initial macroscopic motion of the ***E*-ArF$_2$** crystal is due to the collective evolution of molecular motion initiated by light triggered *E*- to *Z*-isomerization and the [2 + 2] cycloaddition reaction in the solid matrix. The differential packing arrangements (*E*-reactant and *Z*-product) create an interfacial bimorphic strain within the crystal and are responsible for shape deformation. The packing diagram shown in Fig. 4d and S10–S12, ESI† reveals that the ***E*-ArF$_2$** molecules are longitudinally aligned along the width of the crystal (||*c*-axis). When UV light is shone on the (001) face, the molecules on the surface undergo *E*- to *Z*-isomerization which causes a significant decrease in effective molecular length along the

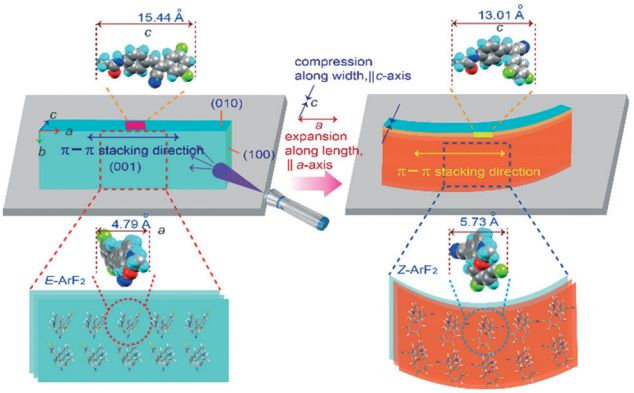

Fig. 6 Mechanistic model of ***E*-ArF_2** actuation by UV illumination. The orientation of ***E*-ArF_2** (viewed along the *c*-axis) was taken from the crystal structure and the arrangement of molecules is shown for representative purposes. The structure of ***Z*-ArF_2** was obtained by manual bond rotation of the ***E*-ArF_2** molecule followed by geometry optimization. The arrangement of ***Z*-ArF_2** molecules is shown as a cartoon for representative purposes.

width of the crystal (||*c*-axis) and a slight increase in effective molecular length along the longitudinal axis of the crystal (||*a*-axis, Fig. 6). These two effects (in the illuminated face where the *cis*-photoproduct concentration is higher) on the molecular scale collectively amplify to the macroscopic scale and causes the shortening of the crystal width and the elongation of the crystal length on the illuminated side (001) and as a result it bends away from the light source. The same mechanism happens when light is shone on the opposite face and the bending occurs in the opposite direction with respect to the illumination direction (as shown in Fig. 3a–g and Movies S6–S8, ESI†). The π–π stacking interactions of the phenyl rings along the length of the crystal (||*a*-axis) retain the crystal integrity during bending, however after repeated and prolonged UV illumination the [2 + 2] cycloaddition reaction occurs which destroys the π–π stacking interaction and as a result the crystal integrity deteriorates and the long range molecular order is diminished. As observed from PXRD (Fig. 5c), the long-range order of the molecules also diminished due to the formation of a mixture of photoproducts (geometric isomers, cycloaddition products, *etc.*) upon prolonged irradiation which could be the possible reason why the crystal stops actuation after a few cycles.

Conclusions

In conclusion, we have demonstrated a light-fueled macroscopic actuator that displays various types of shape deformation that can be controlled remotely in an on-demand fashion using UV light. More importantly, our light-powered actuator has the capability to optically reconfigure to reverse the direction of the movement when the irradiation direction is reversed. With the aid of NMR, IR and X-ray diffraction studies, we have developed a mechanistic model that might be applicable to other molecular systems that show similar photo-actuation behaviour. In addition to optomechanical behaviour, the same crystal emits green fluorescence. Examples of such dual responsive materials (optical and mechanical response) under a single stimulus (light) are extremely rare. These smart materials have immense potential to be utilized in various technological tools in artificial limbs, medicinal equipment, and soft robotics applications.

Conflicts of interest

The authors declare no conflict of interest regarding this work.

Acknowledgements

M. K. P. thanks the UGC, New Delhi, India for start-up research grant (No. F.30-530/2020(BSR)) and SERB India for start-up research grant (F. No. SRG/2020/000943). MKP thanks Jadavpur University for providing basic infrastructure facility. PG, DD, and SG thank the Council for Scientific and Industrial Research (CSIR), New Delhi for fellowship.

Notes and references

1 P. Naumov, D. P. Karothu, E. Ahmed, L. Catalano, P. Commins, J. M. Halabi, M. B. Al-Handawi and L. Li, *J. Am. Chem. Soc.*, 2020, **142**, 13256–13272.
2 L. Zhang, H. Liang, J. Jacob and P. Naumov, *Nat. Commun.*, 2015, **6**, 7429, DOI: 10.1038/ncomms8429.
3 S. C. Sahoo, N. K. Nath, L. Zhang, M. H. Semreen, T. H. Al-Tel and P. Naumov, *RSC Adv.*, 2014, **4**, 7640–7647.
4 D. P. Karothu, J. L. Weston, I. T. Desta and P. Naumov, *J. Am. Chem. Soc.*, 2016, **138**, 13298–13306.
5 M. K. Panda, R. Centore, M. Causà, A. Tuzi, F. Borbone and P. Naumov, *Sci. Rep.*, 2016, **6**, 29610, DOI: 10.1038/srep29610.
6 G. Liu, J. Liu, Y. Liu and X. Tao, *J. Am. Chem. Soc.*, 2014, **136**, 590–593.
7 M. Singh, S. Bhandary, R. Bhowal and D. Chopra, *CrystEngComm*, 2018, **20**, 2253–2257.
8 R. Samanta, S. Ghosh, R. Devarapalli and C. M. Reddy, *Chem. Mater.*, 2018, **30**, 577–581.
9 R. Medishetty, A. Husain, Z. Bai, T. Runčevski, R. E. Dinnebier, P. Naumov and J. J. Vittal, *Angew. Chem., Int. Ed.*, 2014, **53**, 1–6.
10 S. Ghosh, M. K. Mishra, S. Ganguly and G. R. Desiraju, *J. Am. Chem. Soc.*, 2015, **137**, 9912–9921.
11 B. B. Rath and J. J. Vittal, *J. Am. Chem. Soc.*, 2020, **142**, 20117–20123.
12 B. B. Rath, G. Gallo, R. E. Dinnebier and J. J. Vittal, *J. Am. Chem. Soc.*, 2021, **143**, 2088–2096.
13 A. Takanabe, M. Tanaka, K. Johmoto, H. Uekusa, T. Mori, H. Koshima and T. Asahi, *J. Am. Chem. Soc.*, 2016, **138**, 15066–15077.
14 N. K. Nath, T. Runčevski, C.-Y. Lai, M. Chiesa, R. E. Dinnebier and P. Naumov, *J. Am. Chem. Soc.*, 2015, **137**, 13866–13875.

15 S. Li and D. Yan, *ACS Appl. Mater. Interfaces*, 2018, **10**, 22703–22710.
16 S. Kobatake, S. Takami, H. Muto, T. Ishikawa and M. Irie, *Nature*, 2007, **446**, 778–781.
17 M. Morimoto and M. Irie, *J. Am. Chem. Soc.*, 2010, **132**, 14172–14178.
18 F. Terao, M. Morimoto and M. Irie, *Angew. Chem., Int. Ed.*, 2012, **51**, 901–904.
19 P. Naumov, S. Chizhik, M. K. Panda, N. K. Nath and E. Boldyreva, *Chem. Rev.*, 2015, **115**, 12440–12490.
20 T. Kim, L. Zhu, R. O. Al-Kaysi and C. J. Bardeen, *ChemPhysChem*, 2014, **15**, 400–414.
21 J. M. Halabi, E. Ahmed, S. Sofela and P. Naumov, *Proc. Natl. Acad. Sci. U. S. A.*, 2021, **118**, e2020604118, DOI: 10.1073/pnas.2020604118.
22 L. Gao, Y. Hao, X. Zhang, X. Huang, T. Wang and H. Hao, *CrystEngComm*, 2020, **22**, 3279–3286.
23 O. S. Bushuyev, T. A. Singleton and C. J. Barrett, *Adv. Mater.*, 2013, **25**, 1796–1800.
24 Y. Ye, L. Gao, H. Hao, Q. Yin and C. Xie, *CrystEngComm*, 2020, **22**, 8045–8053.
25 H. Koshima and N. Ojima, *Dyes Pigm.*, 2012, **92**, 798–801.
26 F. Tonga, M. Al-Haidar, L. Zhu, R. O. Al-Kaysi and C. J. Bardeen, *Chem. Commun.*, 2019, **55**, 3709–3712.
27 H. Koshima, H. Uchimoto, T. Taniguchi, J. Nakamura, T. Asahi and T. Asahi, *CrystEngComm*, 2016, **18**, 7305–7310.
28 T. Kim, L. Zhu, L. J. Mueller and C. J. Bardeen, *J. Am. Chem. Soc.*, 2014, **136**, 6617–6625.
29 H. Koshima, R. Matsuo, M. Matsudomi, Y. Uemura and M. Shiro, *Cryst. Growth Des.*, 2013, **13**, 4330–4337.
30 H. Koshima, K. Takechi, H. Uchimoto, M. Shiro and D. Hashizume, *Chem. Commun.*, 2011, **47**, 11423–11425.
31 R. Mandal, A. Garai, S. Peli, P. K. Datta and K. Biradha, *Chem. – Eur. J.*, 2020, **26**, 396–400.
32 Y. Shu, K. Ye, Y. Yue, J. Sun, H. Wang, J. Zhong, X. Yang, H. Gao and R. Lu, *CrystEngComm*, 2021, DOI: 10.1039/D1CE00086A.
33 J. Peng, K. Ye, C. Liu, J. Sun and R. Lu, *J. Mater. Chem. C*, 2019, **7**, 5433–5441.
34 J.-K. Sun, W. Li, C. Chen, C.-X. Ren, D.-M. Pan and J. Zhang, *Angew. Chem., Int. Ed.*, 2013, **52**, 1–6.
35 H. Wang, P. Chen, Z. Wu, J. Zhao, J. Sun and R. Lu, *Angew. Chem.*, 2017, **129**, 9591–9595.
36 F. Tong, W. Xu, T. Guo, B. F. Lui, R. C. Hayward, P. Palffy-Muhoray, R. O. Al-Kaysi and C. J. Bardeen, *J. Mater. Chem. C*, 2020, **8**, 5036–5044.
37 D. Kitagawa and S. Kobatake, *Chem. Commun.*, 2015, **51**, 4421–4424.
38 D. Kitagawa, K. Kawasaki, R. Tanaka and S. Kobatake, *Chem. Mater.*, 2017, **29**, 7524–7532.
39 A. Ryabchun, Q. Li, F. Lancia, I. Aprahamian and N. Katsonis, *J. Am. Chem. Soc.*, 2019, **141**, 1196–1200.
40 P. Gupta, T. Panda, S. Allu, S. Borah, A. Baishya, A. Gunnam, A. Nangia, P. Naumov and N. K. Nath, *Cryst. Growth Des.*, 2019, **19**, 3039–3044.
41 P. Li, J. Wang, P. Li, L. Lai and M. Yin, *Mater. Chem. Front.*, 2021, **5**, 1355–1363.
42 L. Zhu, F. Tong, N. Zaghloul, O. Baz, C. J. Bardeen and R. O. Al-Kaysi, *J. Mater. Chem. C*, 2016, **4**, 8245–8252.
43 F. Tong, D. Kitagawa, I. Bushnak, R. O. Al-Kaysi and C. J. Bardeen, *Angew. Chem., Int. Ed.*, 2021, **60**, 2414–2423.
44 Z. Wu, S. Mo, L. Tan, B. Fang, Z. Su, Y. Zhang and M. Yin, *Small*, 2018, **14**, 1802524.
45 X. Luo, J. Li, C. Li, L. Heng, Y. O. Dong, Z. Liu, Z. Bo and B. Z. Tang, *Adv. Mater.*, 2011, **23**, 3261–3265.
46 G. M. J. Schmidt, *Pure Appl. Chem.*, 1971, **27**, 647–678.
47 K. Biradha and R. Santra, *Chem. Soc. Rev.*, 2013, **42**, 950–967.